

Generation of optical beams with desirable orbital angular momenta by transformation media

Weixing Shu, Dongmo Song, Zhixiang Tang, Hailu Luo,

Youngang Ke, Xiaofang Lü, Shuangchun Wen,* and Dianyuan Fan

*Key Laboratory for Micro-/Nano-Optoelectronic Devices of Ministry of Education,
College of Information Science and Engineering, Hunan University, Changsha 410082, China*

We propose a scheme to controllably convert the wavefront of an arbitrary incident beam into a helical one by compact transformation slabs, thus enabling the output beam to carry desirable orbital angular momentum (OAM). First, based on transformation optics, a three-dimensional (3D) phase transformation between any two wavefronts by flat transformation media is established and then used to mold a wavefront of Gaussian beam into a helical one. Second, 3D FDTD simulations are performed to confirm the spiraling evolutions of the resultant field and phase, clearly demonstrating OAM generated. Further theoretical analyses show that the refractive index exhibiting a helical distribution leads to the oppositely spiral phase front and that it is feasible to produce desirable OAM by generators of unit OAM. The results not only provide an additional way to manipulate phase and photon OAM, but reciprocally shed further light on the phase structure of helical beams, which leads to a new transformation way by a surface.

PACS numbers: 42.50.Tx, 42.15.Dp, 42.25.Bs, 78.67.-n

Keywords: helical wavefront, orbital angular momentum, phase transformation, transformation optics

I. INTRODUCTION

Phase is an important characteristic of electromagnetic waves. As well known a beam with a phase $\exp(i l \theta)$ depending on the azimuthal angle θ and an integer l , typically Laguerre-Gaussian (LG) mode, possesses helical wavefront or optical vortex. It thus has an azimuthal component to the linear momentum, resulting in an orbital angular momentum (OAM) of $l\hbar$ per photon along the beam axis [1–3]. Owing to its fascinating properties, the beam has received a great deal of attention [4–6] and has brought novel applications in manipulating particles [7] or atoms [8], classical [9] or quantum communication [10], imaging [11], optical data storage [12] as well as biophysics [13]. Among the usual methods to produce helical beams: mode converters require specific input modes [1]; spiral phase plates have special profiles difficult to fabricate especially in optical frequencies and to obtain high quality beam [14, 15]; computer-generated holograms similar to diffraction gratings have limited conversion efficiency and mode purity [16]; spatial light modulators made of liquid crystal pixels are a tunable generation way, yet need be electronically driven [3]. The last two require low input power as well.

To harness phase, transformation optics that allows the control of waves in a desirable way provides a promising route [17]. It translates electromagnetic behaviors wanted into the distribution of material parameters that are then implemented by transformation media, usually metamaterials [18]. This controllable method provides great flexibility in designing optical devices and a variety of exciting functions have been proposed [19, 20]. To manipulate phase recent work realized field rotation [21]

and directive emission that has important applications such as highly directive antennas [22–26]. The latter was achieved by transforming curved waves into plane ones directly. That transformation way leads to devices with irregular profiles to perform the conversion between curved waves [27] or even between a plane wave and another one deflected [28]. However, flat configurations are preferred in practical applications, especially as plug-and-play devices, being compact enough and free of aberrations [29]. To obtain flattened devices further transformations need be carried on geometrical shapes [30, 31]. Instead we proposed to directly accomplish phase conversion between waves by flat transformation media [32].

According to Fermat's principle the distribution of refractive index determines the generated wave phase [33]. So far, metamaterials of refractive index ranging from positive to negative or from high to zero have been fabricated successfully [34, 35], while transformation optics permit to manipulate phase exactly. By combining them it is hence possible to convert any input modes into pure helical ones of any orbital angular momenta (OAMs). Moreover, the large range of material parameters available will make the design ultra-compact whereby generating desirable OAMs as conveniently and economically as plug-and-play devices.

In this work we hence propose a controllable scheme based on transformation optics to produce helical phase fronts by compact flat configurations. We first put forward a method of three-dimensional (3D) transformation between any two wavefronts and use it to shape the helical wavefront out of Gaussian beam. Next we perform 3D FDTD simulations to reveal the physical process and confirm the generation of OAM. The phase structure of light beams with OAM are examined from the viewpoint of transformation optics, which leads to a new transformation way by a surface. Further we propose available materials to realize the design and demonstrate to pro-

*scwen@hnu.edu.cn

duce arbitrary OAMs tunably using generators of unit OAM. The device is theoretically reflectionless because the 3D transformation achieves the impedance match [36], so the conversion efficiency is high. If proper materials employed the slab may support high intensity beam.

II. PRINCIPLE

A. Light beam with helical wavefronts

For an initially Gaussian-enveloped beam bearing OAM, the field is an eigenmode of the paraxial Helmholtz equation [1–3]:

$$E_l(r, \theta, z) = E_0 \frac{w_0}{w} \left(\frac{r}{w}\right)^{|l|} \exp\left(\frac{-r^2}{w^2}\right) \exp[-i\Phi(r, \theta, z)] \quad (1)$$

where E_0 is the amplitude parameter, w_0 is the waist radius, the beam width $w = w_0 \sqrt{1 + (z/z_R)^2}$, the Rayleigh length $z_R = \pi w_0^2/\lambda$, the wavenumber $k = 2\pi/\lambda$, λ denotes the vacuum wavelength, the phase

$$\Phi(r, \theta, z) = -(|l| + 1) \tan^{-1} \frac{z}{z_R} + \frac{kr^2}{2R(z)} + l\theta + kz, \quad (2)$$

and $R(z) = z + z_R^2/z$ is the wavefront radius of curvature. This is actually LG_0^l mode that reduces to a fundamental Gaussian beam when $l = 0$ [1]. In Eq. (2) the first term and $R(z)$ are relatively slowly varying functions and are effectively constants within the beam width on each wavefront. Then the equiphase surface, $z = g_H(r, \theta) = c_H - r^2/2R - l\theta/k$, defines a helix circling the z -axis with a pitch of $l\lambda$, while with a radius of curvature R for a fixed θ . Meanwhile the wavefront of Gaussian beam $z = g_G(r, \theta) = c_G - r^2/2R$ is a paraboloidal surface and c_H and c_G are constants. As shown in Fig. 1 the above green helicoid corresponds to helical beam with l , while the low blue surface Gaussian beam.

B. 3D phase transformation method by slabs

To convert an arbitrary wavefront into another, e.g. $z = g_G$ into $z = g_H$, one can transform points on the former into the latter immediately (e.g., $A \rightarrow B$). The phase difference added is $k(g_H - g_G)$. Such an intuitive and direct method, however, leads to the device with an irregular shape [27]. Alternatively we introduce a new way in this work and consider a flat cylindrical design of length d and radius r_0 . We find that if a profile of the distance between the two wavefronts is transformed into a plane surface $z = d$ (e.g., $C \rightarrow D$), the phase difference introduced equals $k[d - (g_G - g_H)]$, the same as the former except a constant which will not affect the phase profile. According to the principle of equal optical path length [33], the two transformation ways will generate the same wavefront, whereas the latter results in a

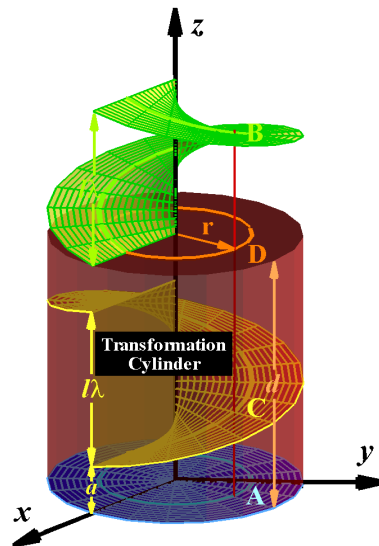


FIG. 1: (color online). Schematic of the coordinate transformation upon which the resultant transformation cylinder converts a wavefront of Gaussian beam into a helical one. The common way is to transform the former (bottom blue surface) into the latter (top green helicoid) directly, i.e. $A \rightarrow B$, whereby the resultant device has an irregular profile. Alternatively we employ a new way that is to transform a surface (lower yellow helicoid) opposite to the wavefront desired (green helicoid) into a plane (upper red surface), i.e. $C \rightarrow D$, which leads to a flat cylinder.

flat transformation medium [32]. The 3D transformation may be written as

$$r' = r, \quad \theta' = \theta, \quad z' = dz/\Delta, \quad (3)$$

where $\Delta = g_G - g_H$ refers to the spatial separation. Following transformation optics [17] the permittivity and permeability tensors of the transformed medium $\boldsymbol{\varepsilon}$ and $\boldsymbol{\mu}$ are respectively related to the original $\boldsymbol{\varepsilon}_o$ and $\boldsymbol{\mu}_o$ by $\boldsymbol{\varepsilon} = \Lambda \boldsymbol{\varepsilon}_o \Lambda^T / \det(\Lambda)$ and $\boldsymbol{\mu} = \Lambda \boldsymbol{\mu}_o \Lambda^T / \det(\Lambda)$ where Λ is the Jacobian matrix between the transformed and original coordinates. Upon the above transformation we obtain for the cylinder

$$\boldsymbol{\varepsilon}(\boldsymbol{\mu}) = \begin{bmatrix} \frac{\Delta}{d} & 0 & 0 \\ 0 & \frac{\Delta}{d} & -\frac{z\Delta'}{dr} \\ 0 & -\frac{z\Delta'}{dr} & \frac{d}{\Delta} + \frac{z^2\Delta'^2}{dr^2\Delta} \end{bmatrix}, \quad (4)$$

where $\Delta' = \partial\Delta/\partial\theta$ and the original space is vacuum.

C. Application to produce helical beam

Applying the above method we convert an incident wavefront g_G located at $z = a$ into the exit one g_H twisting in the $-\hat{\theta}$ direction with a phase variation $2\pi l$ in one around. Then $\Delta = a + l\theta/k$, the surface spiraling in the $\hat{\theta}$ direction (middle yellow helicoid), is to be transformed into a plane surface $z = d$ (top red surface). Here the virtual space is the domain below the helicoid, whereas the

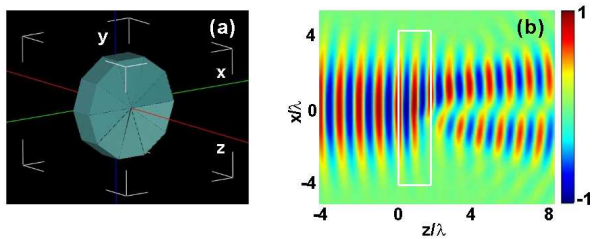


FIG. 2: (color online). (a) Discrete model to simulate. (b) Normalized field magnitude across the longitudinal section of the cylinder.

physical space is the cylinder [37, 38]. For convenience we rewrite the above results in the Cartesian coordinate system $Oxyz$. The transformation now becomes

$$x' = x, y' = y, z' = 2\pi z / (n\theta + 2\pi m), \quad (5)$$

where $\theta = \tan^{-1}(y/x)$ is the azimuth angle in the Oxy plane, $n = l\lambda/d$ and $m = a/d$. Note that a related to the initial point coordinate is introduced to avoid singular points in $\varepsilon(\boldsymbol{\mu})$. Because the transformation is carried out in the z direction, it is feasible to consider the longitudinal coordinate independent of transverse ones, leading to anisotropy reduced greatly [37, 38]. Then Eq. (4) becomes diagonal,

$$\varepsilon(\boldsymbol{\mu}) = \text{diag} \left[m + \frac{n\theta}{2\pi}, m + \frac{n\theta}{2\pi}, \frac{2\pi}{n\theta + 2m\pi} \right]. \quad (6)$$

As a result, the impedance match is achieved on the boundary, so the cylinder can be regarded reflectionless [36] and the conversion efficiency will be high.

III. NUMERICAL CONFIRMATION

A. Transverse field and phase

We now perform numerical simulations to validate the theoretical results and to reflect the physical process involved using the 3D finite-difference time-domain (FDTD) methods [39]. Consider a y -polarized Gaussian beam with $w_0 = 2\lambda$ normally incident on a cylinder of $d = 2\lambda$, $r_0 = 4\lambda$, $a = 2\lambda$, and $l = 1$. We take $\lambda = 1500\text{nm}$ for the sake of simplicity and feasible implementation [40, 41]. Considering practical realization, the cylinder is divided into 10 sectors of discrete $\varepsilon(\boldsymbol{\mu})$ as illustrated in Fig. 2(a). The field distribution in the longitudinal section across $\theta = 0$ and π is shown in Fig. 2(b). Apparently the outgoing field vanishes along the propagation axis indicating a phase singularity, a characteristic inherent to helical beams [4]. One can see that a/λ equals the period number of wave in the lower section $\theta = 0$. Although it may affect the constitutive parameters and the field within the cylinder, a would not change the output field or OAM.

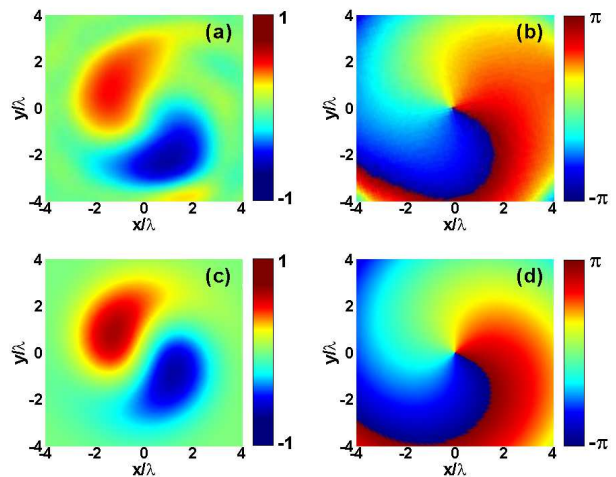


FIG. 3: (color online). Transverse (a) field and (b) phase distributions of the transmitted beam 5λ away from the exit surface. (c) and (d) are the theoretical results determined by Eq. (1) corresponding to (a) and (b), respectively.

Further we show the instantaneous field and phase of the output beam in a cross section in Fig. 3. Apparently the field distribution displays two spiral arms moving anticlockwise. At the same time, a phase change of 2π occurs in a clockwise round. That indicates the resultant wavefront consists of $|l| = 1$ helicoid. The simulated results in (a) and (b) agree satisfactorily with the theoretical ones by Eq. (1) in (c) and (d), respectively. So the photon has acquired an \hbar OAM. The OAM does not be generated from nihility, but involves exchange of momenta between the beam and the cylinder, while the total OAMs are conserved. Usually this leads to measurable mechanical consequences [1, 4].

B. Distribution of refractive index

From the above the complex amplitude transmittance of electromagnetic wave through the slab can be written as $t = \exp(-ik\Delta)$ [42]. Then we introduce the effective average refractive index to characterize the slab as usual [37, 38], $n_{eff} = \Delta/d$. It is consistent with $n_{eff} = \sqrt{\varepsilon_y \mu_x}$ deduced from Eq. (4) for y -polarization. Using Eq. (6)

$$n_{eff} = m + n \frac{\theta}{2\pi}, \quad (7)$$

so the refraction index is helically distributed, as shown in Fig. 4(a) for the slab in Fig. 2. Obviously the anticlockwise helical n_{eff} gives rise to a clockwise helical phase front in Fig. 3(b) and then an anticlockwise helicity on the ray trajectory in Fig. 3(a), as anticipated. The azimuthal distribution of n_{eff} for different choices of a is shown in (b) where the dashed line corresponds to the slab in Fig. 2. It shows that n_{eff} increases with a , i.e. the extent of coordinate compression. Accordingly the choice of transformations determines whether n_{eff} or $\varepsilon(\boldsymbol{\mu})$ are high or low, positive or negative, or near zero.

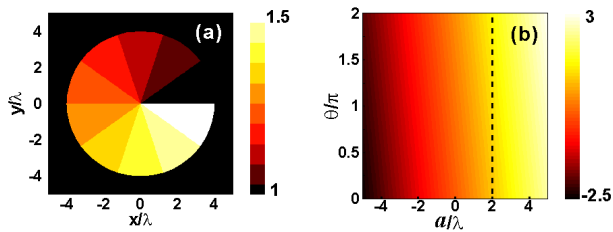


FIG. 4: (color online). Refraction index distribution (a) in the transverse section and (b) around the circumference for different a .

C. Physical process of OAM generation and the phase structure of helical beam

The underlying physics of OAM generation can be studied even further by viewing the movies S1 to S3, corresponding to Fig. 2, Fig. 3(a) and (b), respectively [43]. S1: As the wave propagate through the cylinder, the wavefront begins to advance in the section of larger θ with larger n_{eff} , exhibiting a compression in wavelength. Then a phase difference of $l\pi$ is produced between the upper and lower parts of a longitudinal section, yet the phase on the central z axis becomes undetermined. S2 and S3: Through the cylinder $t = \exp(-ika - i l \theta)$ is imprinted onto the field of the output beam, resulting a helical wavefront. Evolving with time, the output transverse field (S2) and phase (S3) will rotate round z axis. *The transverse phase for any z changes continuously by $2\pi l$ around the beam circumference, while the center is a phase singularity* (we denote this fact by $*$). These results agree with the theory about OAM beams, confirming the above principle based on transformation optics.

Reciprocally the principle from the viewpoint of transformation optics reveals the dynamic phase structure of beams with OAM. Since the wavefront is defined as a equal-phase surface, *there is one wavefront traversing any point of the transverse phase profile* in Fig. 3(b) or S3. Following $*$ each wavefront will rotate, too and undergo a continuous transition into the next sheet after one round trip [2]. Also by the above principle we conclude that *one wavefront is a continuous helicoid with a pitch $l\lambda$* (we denote the two statements in italics by $**$).

It has been pointed out in literature that the wavefront structure is composed from $|l|$ identical helices nested on the beam axis separated by λ [4]. This perception (designated by \ddagger) was adopted in order to interpret the fact (indexed by $*$) that when such a helical beam interferes with a plane wave, it produces a transverse intensity pattern with $|l|$ spiral arms [44]. Now $*$ and $**$ provide an alternative perspective to understand \ddagger . According to $*$ as shown in Fig. 3(b) or S3, there always exist $|l|$ points in-phase with the plane wave wherein arises the total constructive interference [33]. Also due to the azimuthal dependence and the radial curvature of phase, the resultant intensity assumes $|l|$ spiral fringes. Undoubtedly, corresponding to the $|l|$ points there exist $|l|$ wavefronts which

are just those in \ddagger , yet far from the whole. Based upon $*$ and $**$, *the overall wavefronts consist of infinite sequential helicoids with a uniform pitch $l\lambda$ yet individual relative phases in $[0, 2\pi l]$ separated by infinitesimal distance on the beam axis.*

So it is reasonable to adopt a physical picture combining $*$ and $**$ to describe the dynamic structure exactly and concisely, by which one can find two coordinate transformation ways to realize helical beams. This first based on $**$ is to carry 3D space transformation (3DST), which is just the content of the present work. The other based on $*$ means a helical beam can be obtained through a two-dimensional (2D) *surface* transformation (2DST). It indicates that the design also can be implemented by a *surface*. Most recently Yu *et al* produced vortex beam by a 2D array of subwavelength resonators [45]. The 2DST method coincides with their result which followed a different theory though, indicating the 2DST feasible. As being unique the 2DST may become a significant approach to phase transformations, especially to obtain ultra-compact devices. Recently another type of 2D transformation was used to control surface electromagnetic waves [46, 47], which was essentially an application of the 3D transformation to 2D wave problems. By contrast, the 2DST is to control 3D waves by 2D transformation and materials.

D. Generation of arbitrary OAMs and feasible physical realizations

It follows from Eq. (7) that one can realize the same helical beam as Fig. 3 but by isotropic all-dielectric media. To show this result and to demonstrate the flexibility of the compact design, we use two such slabs to generate helical beam with $l = 2$. Similarly n_{eff} takes 10 discrete values. The simulated results are shown in Fig. 5. In (a) the phase in the lower half section is 2π advance against that in the upper part outside the cylinder, coincident with (b). Extra care is required in understanding (c). It seems like the phase consisted of two identical segments from $-\pi$ to π . In fact the phase should evolve continuously with a change 4π in one round according to $*$. The specious appearance in (c) is due to the restriction of the mathematical software on the argument of the complex number which is always between $-\pi$ to π . (b) and (c) agree well with the theoretical results by Eq. (1) for a helical beam with $l = 2$. Thus two pieces of unit OAM generator in (a) have imparted an OAM of $2\hbar$ on the output beam. Meanwhile, we find from simulations that when n_{eff} is discretized more, even into 3 values, helical wavefronts still appear. So the discretization process will not affect the generation of OAM fundamentally, which greatly facilitates the realization of the design. Then one can obtain any OAMs in such a superposing way.

The above refractive index distribution can be realized by a dielectric slab with air columns or vice versa whose size or density determine n_{eff} by the effective medium theory [40, 41]. What's more, if the dielectric medium

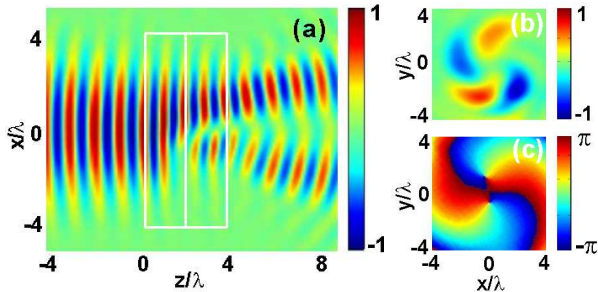


FIG. 5: (color online). Distributions of (a) the field in the longitudinal section of two cylinders, the exit (b) field and (c) phase in the transverse plane 5λ away from the exit surface.

is chosen with a high threshold of damage, e.g. silica, the slab may be able to support high-power beam [15]. Recent developments also make such an OAM generator practically realizable. Metamaterials with material parameters radial, azimuthal and both dependent have been constructed in electromagnetic cloaks [19], field rotation [21] and carpet cloak [40, 41], respectively. Hence, there essentially does not exist technological obstacle to actualize the parameters of Eq. (4). As the loss is inevitable in metamaterials, it affects the amplitude and phase at individual points, but the overall relative phase can be kept helical. So the loss will not prevent the generation of OAM though may affect the quality of beam, as confirmed by additional simulations. Particularly it will be out of question when all-dielectric media are used.

It should be noted that recently a new approach has been proposed to generate OAM beams using inhomogeneous anisotropic media with the configuration very similar to that in Fig. 4 [48]. The media could be implemented by anisotropic crystals [48, 49], liquid crystals [50], or subwavelength gratings [51, 52]. Therein the phase was changed through manipulating the polarization. The added phase results from the so-called Pancharatnam-Berry geometric phase that accompanies space-variant polarization manipulation [51–53]. From the viewpoint of momentum conversion, it is the spin angular momentum of the input beam that is transferred into the OAM of the output beam. In contrast, the method reported here is to transform the phase immediately, without involving the polarization. The phase is introduced through optical phase differences. So the exchange of OAM takes place between the output beam and the transformation medium.

IV. CONCLUSION

In summary, we have shown it is possible to enable a beam to carry OAM employing transformation media. Applying a 3D phase transformation method, we obtain the material parameters with a helical distribution of refraction index. Further 3D FDTD simulations reveal the dynamic process of OAM generation, confirm the theoretical result and manifest the feasibility to obtain any OAMs. The results not only present a new route to accurately produce OAM, but reciprocally reveal the properties of beams bearing OAM. We recognize that it is reasonable to adopt a physical picture combining (*) and (**) to describe the dynamic structure of phase exactly and concisely. Such an understanding allows a helical beam to be obtained by two transformation ways, the 3DST discussed presently and the 2DST which results in a planar device, i.e. implemented by a surface. It is hoped to return to the latter issue elsewhere.

Besides generating OAM beams the cylinder permits to detect a particular OAM state [4, 54]. When operated in reverse, the cylinder for l flattens the helical phase fronts of $-l$ -beam and the output beam, now with planar phase fronts, can be detected. This allows the l value of any helical beam to be measured unambiguously. Further work is desired to experimentally realize the scheme. The transformation method advanced in the present work allows one to tailor a beam's wavefront by flat media in a desirable way and should have practical implications for a wide range of flat optical components. For simplicity we have only considered the longitudinal transformation on wave. If taking into account the transversal expansion/suppression to control the beam dimension [36] or the azimuthal twist to control polarization [55] as well, a more or full control on wave will be achieved.

Acknowledgments

We gratefully acknowledge the referee for his insightful comments and valuable suggestions. This work was supported in part by the National Natural Science Foundation of China (No. 10847121, 10804029, 10904036, 61025024) and the Growth Program for Young Teachers of Hunan University.

-
- [1] L. Allen, M. W. Beijersbergen, R. J. C. Spreeuw, and J. P. Woerdman, *Phys. Rev. A* **45**, 8185 (1992).
 [2] M. S. Soskin, V. N. Gorshkov, M. V. Vasnetsov, J. T. Malos, and N. R. Heckenberg, *Phys. Rev. A* **56**, 4064 (1997).
 [3] J. E. Curtis and David G. Grier, *Phys. Rev. Lett.* **90**, 133901 (2003).

- [4] L. Allen, S. M. Barnett, and M. J. Padgett, *Optical Angular Momentum*, (Institute of Physics Publishing, Bristol, 2003).
 [5] M. S. Soskin and M. V. Vasnetsov, *Prog. Opt.* **42**, 219 (2001).
 [6] A. M. Yao and M. J. Padgett, *Advances in Opt. and Photon.* **3**, 161 (2011).

- [7] D. G. Grier, *Nature* **424**, 810 (2003).
- [8] M. F. Andersen, C. Ryu, P. Cladé, V. Natarajan, A. Vaziri, K. Helmerson, and W. D. Phillips, *Phys. Rev. Lett.* **97**, 170406 (2006).
- [9] G. Gibson, J. Courtial, M. J. Padgett, M. Vasnetsov, V. Pas'ko, S. M. Barnett, and S. Franke-Arnold, *Opt. Express* **12**, 5448 (2004).
- [10] G. Molina-Terriza, J. P. Torres, and L. Torner, *Nature Phys.* **3**, 305 (2007).
- [11] L. Torner, J. P. Torres, S. Carrasco, *Opt. Express* **13**, 873 (2005).
- [12] R. J. Voogd, M. Singh, S. Pereira, A. van de Nes, and J. Braat, *Proceedings of SPIE* **5380**, 387 (2004).
- [13] K. Dholakia and T. Čížmár, *Nature Photon.* **5**, 335 (2011).
- [14] M. W. Beijersbergen, R. P. C. Coerwinkel, M. Kristiansen, and J. P. Woerdman, *Opt. Commun.* **112**, 321 (1994).
- [15] K. Sueda, G. Miyaji, N. Miyanaga, and M. Nakatsuka, *Opt. Express* **12**, 3548 (2004).
- [16] V. Y. Bazhenov, M.S. Soskin, and M.V. Vasnetsov, *J. Mod. Opt.* **39**, 985 (1992).
- [17] J. B. Pendry, D. Schurig, and D. R. Smith, *Science* **312**, 1780 (2006).
- [18] T. J. Cui, D. R. Smith, and R. P. Liu, *Metamaterials: Theory, Design, and Applications* (Springer Science+Business Media, New York, 2010).
- [19] D. Schurig, J. J. Mock, B. J. Justice, S. A. Cummer, J. B. Pendry, A. F. Starr, and D. R. Smith, *Science* **314**, 977 (2006).
- [20] H. Y. Chen, C. T. Chan and P. Sheng, *Nature Mater.* **9**, 387 (2010).
- [21] H. Y. Chen, B. Hou, S. Y. Chen, X. Y. Ao, W. J. Wen, and C. T. Chan, *Phys. Rev. Lett.* **102**, 183903 (2009).
- [22] W. X. Jiang, T. J. Cui, H. F. Ma, X. Y. Zhou, and Q. Cheng, *Appl. Phys. Lett.* **92**, 261903 (2008).
- [23] D.-H. Kwon and D. H. Werner, *New J. Phys.* **10**, 115023 (2008).
- [24] L. Lin, W. Wang, J. Cui, C. L Du, and X. G. Luo, *Opt. Express* **16**, 6815 (2008).
- [25] P.-H. Tichit, S. N. Burokur, D. Germain, and A. de Lustrac, *Phys. Rev. B* **83**, 155108 (2011).
- [26] F. Kong, B. Wu, J. A. Kong, J. Huangfu, and S. Xi, *Appl. Phys. Lett.* **91**, 253509 (2007).
- [27] H. Ma, S. B. Qu, Z. Xu, and J. F. Wang, *Opt. Express* **16**, 22072 (2008).
- [28] G. X. Yu, W. X. Jiang and T. J. Cui, *Cent. Eur. J. Phys.* **9**, 183 (2011).
- [29] N. Kundtz and D. R. Smith, *Nature Mater.*, **9**, 129 (2010).
- [30] D. A. Roberts, N. Kundtz, and D. R. Smith, *Opt. Express* **17**, 16535 (2009).
- [31] R. Yang, W. X. Tang, Y. Hao, and I. Youngs, *IEEE Antennas Wireless Propag. Lett.* **10**, 99 (2011).
- [32] Y. Ke, W. Shu, H. Luo, S. Wen, and D. Fan, *J. Europ. Opt. Soc. Rap. Public.* **7**, 12013 (2012).
- [33] E. Hecht, *Optics*, 4th ed. (Addison-Wesley, San Francisco, 2002).
- [34] I. C. Khoo, D. H. Werner, X. Liang, A. Diaz, and B. Weiner, *Opt. Lett.* **31**, 2592 (2006).
- [35] A. Pimenov and A. Loidl *Phys. Rev. B* **74**, 193102 (2006).
- [36] C. D. Emiroglu and D.-H. Kwon, *J. Appl. Phys.* **107**, 084502 (2010).
- [37] J. Li and J. B. Pendry, *Phys. Rev. Lett.* **101**, 203901 (2008).
- [38] W. X. Tang, C. Argyropoulos, E. Kallos, W. Song, and Y. Hao, *IEEE Trans. Antennas Propag.* **58**, 3795-3804 (2010).
- [39] EastFDTD V3.0, DONGJUN Information Technology Co., Ltd..
- [40] J. Valentine, J. Li, T. Zentgraf, G. Bartal and X. Zhang, *Nature Mater.* **8**, 568 (2009).
- [41] L. H. Gabrielli, J. Cardenas, C. B. Poitras and M. Lipson, *Nature Photon.* **3**, 461 (2009).
- [42] J. W. Goodman, *Introduction to Fourier Optics* (McGraw-Hill Companies, San Francisco, 1996).
- [43] See Supplemental Material at [URL will be inserted by publisher] for the generation of OAM.
- [44] M. Padgett, J. Courtial, and L. Allen, *Phys. Today* **57**, 35 (2004).
- [45] N. F. Yu, P. Genevet, M. A. Kats, F. Aieta, J.-P. Tetienne, F. Capasso, and Z. Gaburro, *Science* **334**, 333 (2011).
- [46] P. A. Huidobro, M. L. Nesterov, L. Martín-Moreno, and F. J. García-Vidal, *Nano Lett.* **10**, 1985 (2010).
- [47] Y. Liu, T. Zentgraf, G. Bartal, and X. Zhang, *Nano Lett.* **10**, 1991 (2010).
- [48] G. Machavariani, Y. Lumer, I. Moshe, A. Meir, and S. Jackel, *Opt. Commun.* **281**, 732 (2008).
- [49] A. Volyar, V. Shvedov, T. Fadeyeva, A. S. Desyatnikov, D. N. Neshev, W. Krolikowski, and Y. S. Kivshar, *Opt. Express* **14**, 3724 (2006).
- [50] L. Marrucci, C. Manzo, and D. Paparo, *Phys. Rev. Lett.* **96**, 163905 (2006).
- [51] G. Biener, A. Niv, V. Kleiner, and E. Hasman, *Opt. Lett.* **27**, 1875 (2002).
- [52] A. Niv, G. Biener, V. Kleiner, and E. Hasman, *Opt. Commun.* **251**, 306 (2005).
- [53] G. Milione, S. Evans, D. A. Nolan, and R. R. Alfano, *Phys. Rev. Lett.* **108**, 190401 (2012).
- [54] G. Weihs and A. Zeilinger, *Nature* **412**, 313 (2001).
- [55] D. H. Kwon and D. H. Werner, *Opt. Express* **16**, 18731 (2008).